

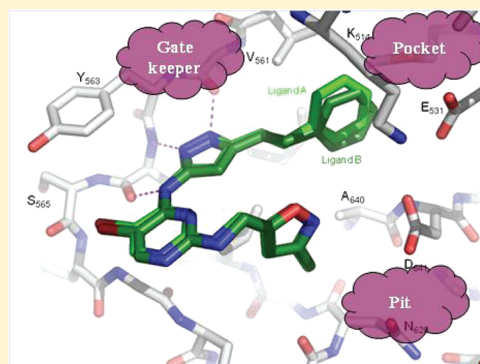
Protein–Ligand Crystal Structures Can Guide the Design of Selective Inhibitors of the FGFR Tyrosine Kinase

Richard A. Norman, Anne-Kathrin Schott, David M. Andrews, Jason Breed, Kevin M. Foote, Andrew P. Garner, Derek Ogg, Jonathon P. Orme, Jennifer H. Pink, Karen Roberts, David A. Rudge, Andrew P. Thomas, and Andrew G. Leach*

AstraZeneca Pharmaceuticals, Mereside, Alderley Park, Macclesfield, SK10 4TG, U.K.

S Supporting Information

ABSTRACT: The design of compounds that selectively inhibit a single kinase is a significant challenge, particularly for compounds that bind to the ATP site. We describe here how protein–ligand crystal structure information was able both to rationalize observed selectivity and to guide the design of more selective compounds. Inhibition data from enzyme and cellular screens and the crystal structures of a range of ligands tested during the process of identifying selective inhibitors of FGFR provide a step-by-step illustration of the process. Steric effects were exploited by increasing the size of ligands in specific regions in such a way as to be tolerated in the primary target and not in other related kinases. Kinases are an excellent target class to exploit such approaches because of the conserved fold and small side chain mobility of the active form.



■ INTRODUCTION

It has become apparent over recent years that selective inhibition of a single kinase is a significant challenge.^{1–4} Several surveys of kinase inhibition profiles and correspondence (or lack of it) with overall sequence, or just binding site sequence, demonstrate the challenges involved in achieving selectivity.^{2,5–11} The so-called gatekeeper residue is often highlighted as a key determinant of selectivity.^{2–4,7,10–14} Such surveys do not provide a route map for how to get from a given compound, or set of compounds, with a given profile to a more selective profile, should that be desired. A compound's selectivity profile depends upon the detail of the interactions of that compound with each binding site.^{2,11} Crystal structures of the protein–ligand complex can provide insight and understanding.^{5,7,15} Such structures are particularly powerful for addressing the issue of selectivity among kinases because of the remarkable degree of conservation of the protein fold among the various kinases.⁷ This similarity means that the structure of a ligand in complex with its desired target kinase in combination with the crystal structure of a second kinase or a sequence alignment with a second kinase can provide insights into how the ligand might be achieving selectivity and further might suggest structural changes to the ligand that would improve the selectivity. Some inhibitors that achieve selectivity rely upon covalent bonding to their target which can make it more difficult to obtain safe and orally bioavailable compounds.¹⁰ Others rely upon variations in the degree of protein flexibility, which remains difficult to predict a priori.^{5,10} In the work reported here, we describe how protein–ligand crystal structure information was used to rationalize observed

selectivity between FGFR1, IGF1R, and KDR to guide the design of more selective FGFR1 inhibitors.

During the course of routine screening of compounds from the AstraZeneca compound collection against a panel of kinase assays (employing the activated enzymes), a small number of pyrazolylaminopyrimidines that inhibited FGFR1 more potently than any of the other kinases in the panel was identified. A lead identification campaign was initiated with the aim of identifying a compound that was sufficiently selective to provide clear evidence for FGFR driven effects in *in vivo* studies. The relative merits of “clean” kinase inhibitors that selectively inhibit one kinase and broad spectrum inhibitors that inhibit many are a subject of vigorous discussion focused particularly around the generally perceived trade-off between efficacy and tolerability.¹⁶ In this case, these starting points had marginal selectivity compared to KDR and were closely related to compounds that were potent inhibitors of IGF1R, the target against which these compounds were originally designed.¹⁷ Plots of potency for inhibiting these two kinases versus that for FGFR1 for the whole series of pyrazolylaminopyrimidines available at the initiation of this program are shown in Figure 1. FGFR1 has been linked to a number of tumor types including bladder cancers and represents an attractive target for medicinal chemistry efforts.¹⁸ With this in mind, a crystal structure for a complex of FGFR1 with one of the initial compounds that had prominent FGFR1 inhibition was sought.

Received: November 15, 2011

Published: May 21, 2012

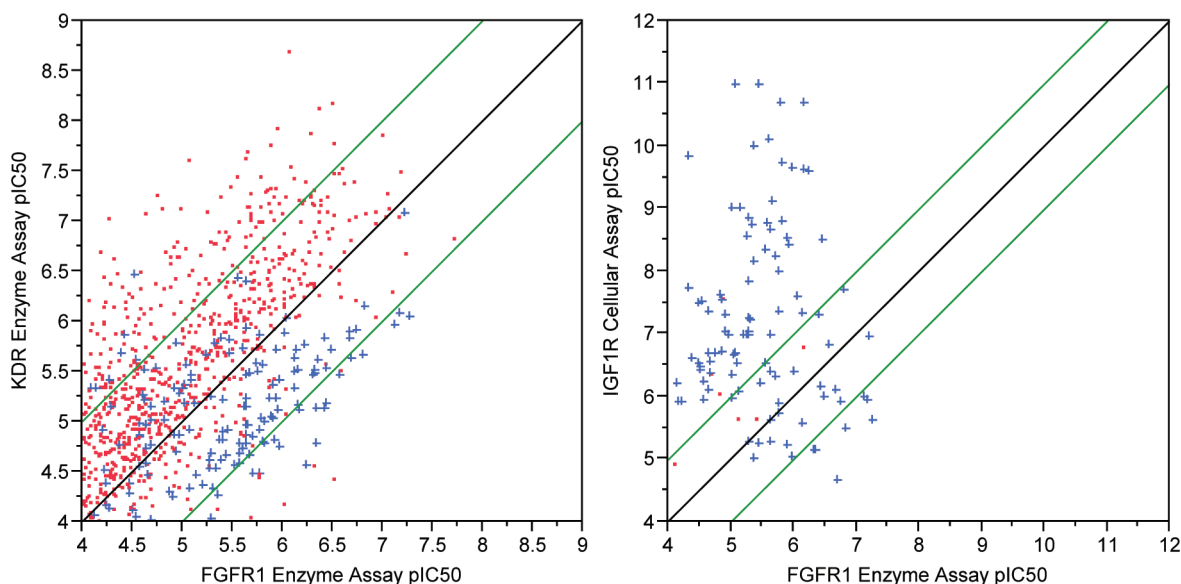


Figure 1. Data from an isolated enzyme assay for KDR (left) and cellular assay for IGF1R (right) are plotted against the corresponding values in an isolated enzyme assay for FGFR1. This is the data set that was available at the initiation of a program to identify and design selective inhibitors of FGFRs. The pIC_{50} ($-\log_{10} IC_{50}$) values for compounds tested against both targets are plotted against one another with pyrazolylaminopyrimidines highlighted as blue + symbols. The black line is the line of equality, with the upper green line indicating the point at which compounds are 10-fold selective for KDR or IGF1R and the lower line indicating 10-fold selectivity for FGFR1.

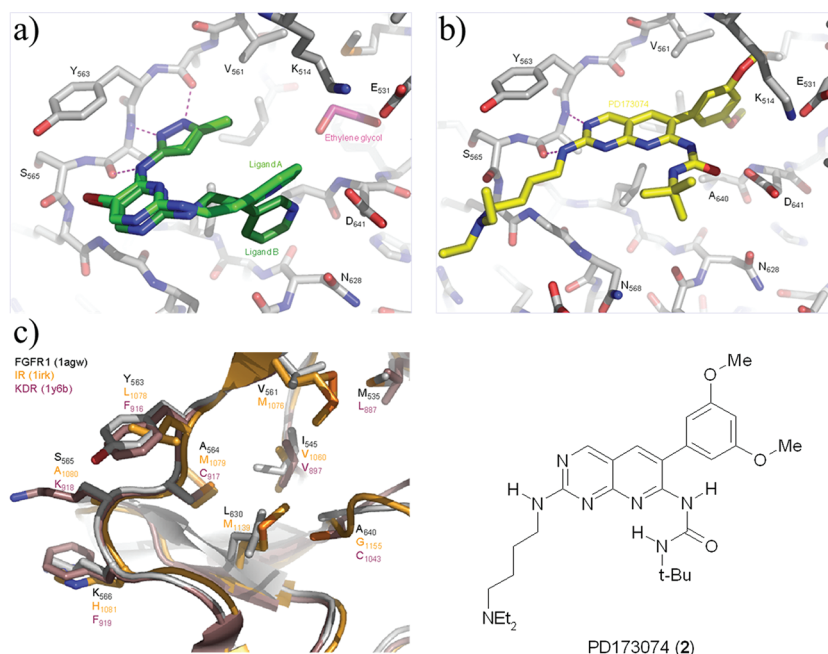
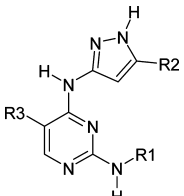


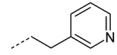
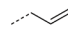
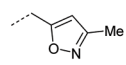
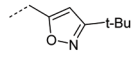
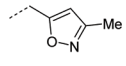
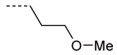
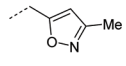
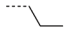
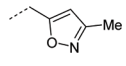
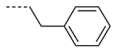
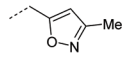
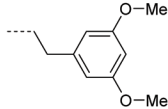
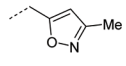
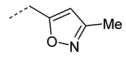
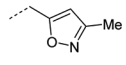
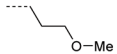
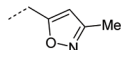
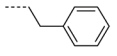
Figure 2. (a) Crystal structure of the complex of **1** with FGFR1. There are two protein–ligand complexes in the asymmetric unit, and the conformations of **1** in both are shown. (b) Crystal structure of PD173074 (**2**) in complex with FGFR1 (PDB accession code 2FGI).¹⁹ (c) Overlaid structures showing key residues surrounding the binding site in FGFR1 (in black, PDB accession code 1AGW),²⁰ InsR (in orange, PDB accession code 1IRK),²¹ and KDR (in purple, PDB accession code 1Y6B).²²

RESULTS AND DISCUSSION

The crystal structure of the complex of pyrazolylaminopyrimidine **1** with the FGFR1 kinase domain is shown in Figure 2a. Details of the construct and methods for obtaining this structure are provided in the Experimental Section. The protein structure is very similar to that observed for two Sugen compounds²⁰ and for a compound originally disclosed by the Parke-Davis company (PD173074 (**2**),^{19,23} also shown in Figure 2b). Compound **1** binds in the ATP site, as also

observed for those compounds. A molecule of ethylene glycol, derived from the cryoprotection buffer, is observed in the structure of **1** that is absent in the public domain structures (Figure 2a). Compound **1** was known to be an equipotent inhibitor of FGFR1 and KDR (compare the fifth and sixth columns in Table 1). The sequence alignment of FGFR1 with KDR provided a “map” of the binding site shown in Figure 2c in which the identity of residues close to the ligand in these two kinases (and also InsR, see below) is indicated. One particular

Table 1. Variation of Enzyme and Cellular Potency with Substituents R1, R2, and R3 As Indicated for Pyrazolylaminopyrimidines^a


Cpd	R1	R2	R3	FGFR1 enzyme	KDR enzyme	IGF1R enzyme	FGFR cell	KDR cell	IGF1R cell	InsR cell
1		Me	Br	6.3 [N]	6.2 [FGH]	5.2 [DEFG]	5.6 [E]	<5 [A]	5.4 [B]	5.3 [CD]
3		Me	Br	6.2 [N]	6.0 [GHI]	5.4 [CDE]	5.5 [E]	6.1 [A]	5.2 [BC]	5.5 [B]
4		Me	Br	7.2 [GHIJ]	6.2 [GH]	5.1 [DEFG]	6.8 [CD]	5.2 [A]	5.2 [BC]	5.1 [D]
5		Me	Br	7.5 [EFG]	5.4 [K]	5.0 [DEFG]	6.8 [CD]	<5 [A]	5.5 [B]	5.4 [BC]
6			Br	7.2 [GHI]	5.9 [GHIJ]	4.7 [FHJ]	6.1 [DE]	<5 [A]	<4.7 [D]	5.1 [D]
7			Br	8.0 [D]	6.8 [BCDE]	6.4 [AB]	7.0 [ABC]	5.2 [A]	6.3 [A]	6.2 [A]
8			Br	8.6 [AB]	7.6 [A]	5.2 [DEFG]	7.2 [ABC]	5.8 [A]	5.0 [CD]	5.6 [B]
9			H	8.7 [A]	7.1 [B]	5.2 [DEG]	>7.8 [A]	5.8 [A]	5.3 [BC]	5.5 [B]
10		Me	Cl	7.5 [EFG]	6.3 [FGH]	5.1 [DEFG]	-	-	-	-
11		Me	H	7.1 [I]	6.0 [GHIJ]	4.9 [EFGH]	-	-	-	-
12			H	7.1 [GHIJ]	5.6 [IJK]	4.5 [HIJK]	-	-	-	-
13			H	8.1	6.9	4.8	-	-	-	-

^aValues given are average pIC₅₀ values (-log₁₀(IC₅₀), see Experimental Section). Letters in brackets beneath each number show results from a Student's *t*-test; compounds that do not share a letter within a column are distinct at 95% confidence.

sequence difference suggested an opportunity to achieve selectivity; Ala640 in FGFR1 is Cys1043 in KDR. The fact that cysteine has a larger side chain than alanine and that this residue lies in a constricted indentation at the base of the ATP pocket, which we have styled the “pit”, suggested that compounds that rigidly protruded in an appropriate direction to fill this space might be able to achieve selectivity. The flexibility of compound **1** is illustrated by the two conformations observed in the two FGFR1–1 complexes in the crystal asymmetric unit (Figure 2a). The NHCH₂CH₂ linker is sufficiently flexible that it can presumably adapt to the different steric environment in the KDR ATP pocket, and hence, this particular ligand is not well suited to exploit the opportunity offered by the “pit” region of the binding site that the pyridyl ring probes. A number of other pyrazolylaminopyrimidines also incorporating 5-methyl substituted pyrazoles had also been screened, and some are highlighted in the first four rows of Table 1. In this table, the initially available enzyme inhibition data for FGFR1 and KDR are supplemented with enzyme data for IGF1R and cellular data for these three kinases as well as for the insulin receptor tyrosine kinase (InsR). Compound **3** provides a reference for compounds that do not protrude into the “pit” at all, the allyl group being too short to reach this site, and clearly shows in both enzyme and cellular assays that, like **1**, it is an equipotent inhibitor of FGFR1 and KDR. The selectivity of two compounds (**4** and **5**) with more rigid groups at the same position as the CH₂CH₂-pyridyl group in **1** was highly suggestive that the difference between FGFR1 and KDR identified in the crystal structure could indeed be used to gain selectivity. Compounds **4** and **5** have one fewer methylene groups between the NH and the aromatic ring compared to **1** and so have one fewer internal degrees of freedom. Compound **4**, which has a methyl group on the oxazole, manages to increase potency against FGFR1 in a way that is not matched by an increase against KDR. When the methyl group is replaced by the substantially larger *tert*-butyl group in **5**, enzyme potency against FGFR1 is maintained but there is a decrease in potency against KDR. This is replicated at the cellular level. To confirm that compounds possessing an oxazole side chain were engendering selectivity in the way hypothesized above, the crystal structure of a related compound, **6** (Table 1), was sought. This compound was selected by virtue of being potent, soluble, and available in sufficient quantity.

The structure of **6** in complex with FGFR is shown in Figure 3. In contrast to compound **1** only one conformation of the pyrimidine 2-substituent is observed in the two molecules of the crystallographic dimer. This supports the hypothesis that this is a more conformationally rigid group. The structure also shows that the methyl on the isoxazole is directed toward the side chain of Ala640, which can be seen in the background, suggesting a beneficial hydrophobic interaction that would also favor this conformation. This interaction is precisely what was hoped for. In KDR the larger cysteine side chain at this position would either require the ligand to adopt a different conformation or require a perturbation of the binding at the hinge (or both), which would carry an energetic penalty disfavoring binding. When the methyl group on the isoxazole is enlarged further as exemplified in compound **5**, the effect becomes more pronounced with a decrease in KDR inhibition potency.

It was hoped that selectivity could be demonstrated against the set of kinases that possess a methionine gatekeeper residue,

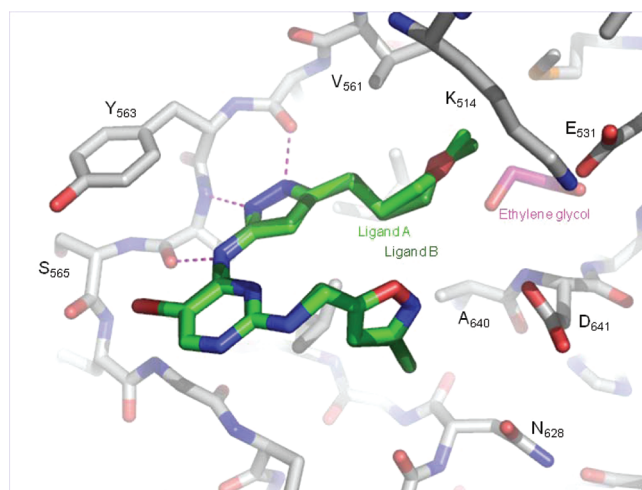


Figure 3. Compound **6** in complex with FGFR1. The conformations of **6** from both molecules in the crystallographic dimer are shown.

which is the second most common gatekeeper residue among tyrosine kinases and the most common across the entire kinome.¹² These include the IGF1R and InsR tyrosine kinases. These two are singled out in particular because in addition to having a Met gatekeeper, they have glycine in place of Ala640 such that the features used to achieve selectivity against KDR would be ineffective against IGF1R and InsR (see Figure 2c). Rather than having less space in the “pit”, they have slightly more. The gatekeeper residue is a well established selectivity handle.^{2–4,7,10–14} The crystal structure of **1** in complex with FGFR1 revealed that the 5-substituent on the pyrazole is directed toward the gatekeeper, Valine 561 in FGFR1. The crystal structure of **2** in complex with FGFR1 shows that the 3,5-dimethoxyphenyl group is positioned such that it is in proximity to the valine side chain. It was our hypothesis that this might not be tolerated by kinases with a methionine gatekeeper. In line with this hypothesis, **2** is reported to have activity of >50 μM against both InsR and MEK, two kinases with a methionine gatekeeper residue.^{19,24} Comparison of the two structures shown in Figure 2a and Figure 2b suggests that if a suitable linker could be found to link the pyrazole that binds at the hinge and an aryl group, a similar effect might be exploited in the pyrazolylaminopyrimidines. It was felt that a two-atom spacer might achieve this, and consequently compound **7** was selected for screening. By good fortune this compound already existed in our compound collection, obviating the need for synthesis. The full data set for compound **6** (used to generate a FGFR1 complex crystal structure) is provided alongside those of **4**, **7**, and **8** which share the same “pit” group in Table 1.

Going from the CH₂CH₂Me group in **7** to the CH₂CH₂Ph group in **8** results in a >0.5 log unit increase in isolated enzyme potency against both FGFR1 and KDR (which has the isosteric Thr gatekeeper). At the same time cellular potency is maintained. By contrast there is a 1.2 log unit decrease in enzyme potency against IGF1R and a >0.5 log unit decrease in cellular potency against the two Met gatekeeper kinases IGF1R and InsR. A feature has been introduced that is tolerated in FGFR1 but not in IGF1R or InsR. If the phenyl group on the CH₂CH₂ spacer had been able to wrap around the gatekeeper, then it could protrude into the hydrophobic pocket occupied snugly by the phenyl ring in **2**. The set of hypotheses, relating binding interactions with desired selectivity, that compound **8**

was selected to test were further probed by obtaining the structure of the complex of **8** with FGFR1 (shown in Figure 4).

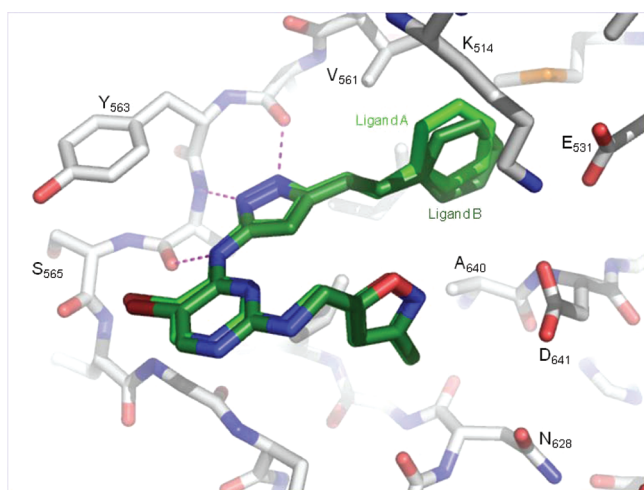


Figure 4. Compound **8** in complex with FGFR1. The conformations of **8** from both molecules in the crystallographic dimer are shown.

The ethylene glycol present in the earlier structures was no longer observed, having presumably been displaced by the phenyl ring. The phenyl group does indeed occupy the hydrophobic pocket, fitting tightly against the gatekeeper,¹² while the methyl isoxazole protrudes into the pit. This indicates that **8** utilizes the various specificity-enhancing features described above.

With encouraging data as presented for compounds **1** and **3–8** in Table 1 and in advance of obtaining the crystal structure shown in Figure 4, it was speculated that replacing the phenyl group in compound **8** with a 3,5-dimethoxyphenyl group, as in **2**, might contribute further to selectivity, as that group was found to fit very snugly into a hydrophobic pocket in the crystal structure shown in Figure 2b. However, the lipophilicity of compound **8** was higher than desired ($\text{clogP} = 4.3$) and was implicated as the cause of a number of problems with the compound,²⁵ including poor solubility. The bromine substituent on the pyrimidine ring was not considered an essential element for FGFR inhibition (see data in Table 1 for compound **10** which is the chloro equivalent of **4** and for compounds **11**, **12**, and **13** which are the des-bromo versions of **4**, **6**, and **8**, respectively), while clearly making a significant contribution to increased lipophilicity (π value for Br is 0.86),²⁶ and so compound **9**, in which this atom was removed and the phenyl ring substituted for 3,5-dimethoxyphenyl, was targeted for synthesis and tested. The outcome of this testing is summarized in Table 1. Compound **9** maintains the same level of inhibition of FGFR in enzyme and cellular assays as **8** while having the same or improved selectivity compared to KDR, IGF1R, and InsR. The FGFR1 potency is particularly striking because the lipophilicity is reduced (clogP for **9** is 3.4) as a result of the removal of the bromine atom and addition of the methoxy groups. The crystal structure of **2** in complex with FGFR1 suggests that one of the two methoxy groups in that compound presses closely against the side chain of Val559 in the hydrophobic pocket. This should entail decreased inhibition of any kinase having a larger group than this at the corresponding position in the sequence. This provides a third point at which steric encumbrance might be used to disfavor binding to kinases other than FGFR. By having two methoxy

groups on the aromatic ring rather than just one, one cannot avoid pushing against Val559.

Compounds **8** and **9** have been tested for inhibition of a larger set of kinases in a single point assay fashion that yields percentage inhibition at a particular concentration. Compound **8** was tested at 10 μM and compound **9** at 1 μM . The percentage inhibition is not a reliable way to quantify selectivity but is a practical way of obtaining a broader view across the kinome. The kinases have been classified according to whether they have larger residues than Ala640, Val 561, and Val559 at the corresponding positions. The mean and range of percentage inhibitions observed for each class are summarized in the two Venn diagrams shown in Figure 5. The three residues targeted

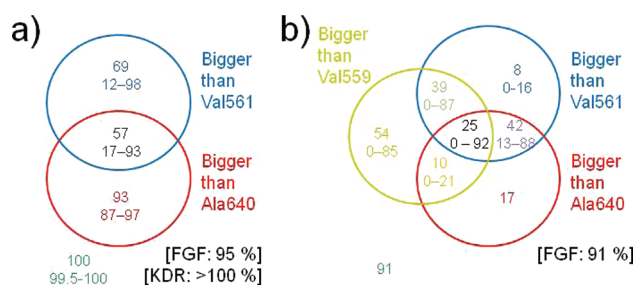
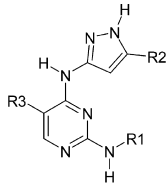
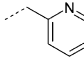
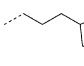
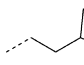
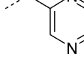
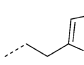
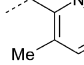
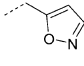
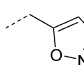
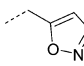
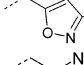
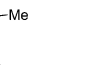
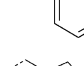
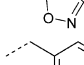
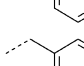
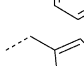
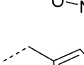
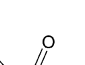
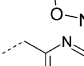
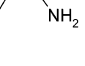
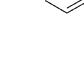

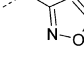
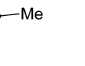


Figure 5. Mean percentage inhibition and the range of percentage inhibition caused by (a) 10 μM **8** and (b) 1 μM **9** against kinases classified according to whether they have a residue larger than Ala640 at the corresponding position (red circle), a residue larger than Val559 at the corresponding position (yellow circle), and a residue larger than Val561 at the corresponding position (blue circle).

in the approach described here could, in principle, permit selectivity against all except 10 kinases, of which six are tyrosine kinases (see Supporting Information for details). Gatekeeper Val561 appears to be the most influential residue, but Ala640 in the pit is also seen to make a useful contribution to diminishing inhibition while Val559 is least influential.

The rationalization of the drivers for selectivity suggested by the crystal structures and probed with enzymatic data permits a more general understanding of the selectivity in the series of pyrazolylaminopyrimidines. With this in mind the compounds in the initial data set shown in Figure 1 have been reanalyzed. A selection of interesting compounds from that set and some tested subsequently that were available in sufficient quantity were selected for screening in the various enzyme assays. Their inhibition values are summarized in Table 2. The series of compounds with Me at R2 (**14–22**) have varying R1 substituents, some of which ought to bind in the “pit”. It is notable that only the cyclopropyl substituted isoxazole **21** binds more tightly to FGFR1 than compound **4**. In line with the hypotheses outlined, **14–22** retain low values of inhibition of KDR and the large amide substituent in **20** is too big to be tolerated in either FGFR or KDR. While it is unsurprising that **21** inhibits FGFR more potently than **4** without an increase in potency against KDR, it is surprising that IGF1R which notionally has a larger “pit” region is not inhibited more strongly. This is consistent with a key role for hydrophobic interactions in the “pit” of FGFR involving the methyl group of the side chain of Ala640. Comparing **14** and **24** shows that increasing the pyrazole 5-substituent from Me to Et increases potency for all three kinases to about the same degree. Compounds **7** and **26** confirm that compared to the 3-pyridyl group the methylisoxazole favors FGFR and IGF1R as

Table 2. Variation of Enzyme Potency with Substituents R1, R2, and R3 As Indicated for Pyrazolylaminopyrimidines^b


Cpd	R1	R2	R3	FGFR1 enzyme	KDR enzyme	IGF1R enzyme
14		Me	Br	6.7 [L]	5.8 [IJ]	4.9 [FH]
15		Me	Br	6.9 [JKL]	6.3 [EFGH]	5.2 [DEFG]
16		Me	Br	6.7 [KLM]	6.7 [BCDEF]	5.4 [CD]
17		Me	Br	7.0 [IJK]	6.0 [GHIJ]	4.9 [EFGH]
18		Me	Br	6.4 [MN]	6.3 [FGH]	4.8 [FGHI]
19		Me	Br	7.1 [HIJ]	6.3 ^a [CDEFGH]	4.3 [JK]
20		Me	Br	5.3 [O]	4.8 [L]	5.0 [DEFGH]
21		Me	H	7.6 [EF]	6.1 [GHI]	5.0 [EFGH]
22		Me	H	7.0 [IJK]	5.9 ^a [GHIJK]	5.1 ^a [DEFG]
23			H	6.1 [N]	4.7 [L]	4.4 [IJK]
24		Et	Br	7.4 [EFGH]	6.3 [FGH]	5.5 [CD]
25		Et	Br	7.1 [HIJ]	5.5 [JK]	7.0 [A]
26		<i>n</i> -Pr	Br	7.6 [E]	6.9 [BC]	5.8 [C]
27		<i>i</i> -Pr	Br	7.2 [FGHIJ]	6.4 [DEFG]	6.4 [B]
28			H	7.6 [EF]	5.8 ^a [HIJK]	4.9 ^a [DEFGHI]
29			H	7.2 [GHIJ]	5.9 [HIJK]	4.0 [K]
30			H	8.3 [BC]	6.4 [EFG]	4.1 [K]
31			H	8.7 [A]	6.9 [B]	4.9 [FGHIJ]

^aData obtained in duplicate only. ^bValues given are average pIC₅₀ (−log₁₀(IC₅₀), see Experimental Section) from at least three measurements other than where indicated. Letters in brackets beneath each number show results from a Student's *t*-test; compounds that do not share a letter within a column are distinct at 95% confidence. The letters designate the same classes as shown in Table 1.

compared to KDR, while **27** suggests that changing *n*-Pr to *i*-Pr enhances potency against IGF1R while reducing it for FGFR

and KDR. The pairs **21+28** and **22+29** present a contrast; changing methyl to methoxypropyl at R2 in **22+29** reduced

IGF1R potency as is observed on going from **4** to **12**, but in **21+28** no change is observed. Compound **30** contrasts markedly to **14** and **24** because its FGFR potency is much higher while KDR remains unchanged and IGF1R declines, recapitulating the particular sensitivity of Met gatekeeper kinases to this structural change. Retention of potency and selectivity for the isoxazole isomer **31** compared to **9** confirms that activity at FGFR1 is not dependent upon the positioning of these heteroatoms.

In conclusion, crystal structures of the complex between a tyrosine kinase and a new lead series have been used to rapidly identify and design compounds that achieve levels of selectivity that are sufficient to allow in vivo testing of specific FGFR-related biological hypotheses. As highlighted by Bamborough et al., it is often the case that gross sequence level similarities, even when localized to the binding pocket, can mask single point differences that are sufficient to permit selective modulation of potency favoring one kinase over another.² How this might be achieved will depend upon the binding mode of the series being developed and therefore requires detailed knowledge of how the protein sequence and different parts of the ligand interact. Crystal structures of appropriate complexes provide just this kind of information. In this case, the steric bulk of three amino acid side chains complemented by a specific hydrophobic interaction has been exploited to gain selectivity. General rules might be difficult or even impossible to derive, requiring detailed consideration of each series and its interactions with each set of kinases. Having crystal structures and high quality enzyme and cellular data for the various stages of the process of tuning selectivity provides a good foundation for believing that the changes measured are caused by the structural changes described. For this particular approach to be successful, the binding mode observed in FGFR1 needs to be energetically favored over the alternative binding modes that a series such as the one described here might adopt. It further requires that the key amino acid side chains are not in positions where they can move freely and at small energetic cost. Kinases in their active form present a well conserved fold and most of the side chains in the ATP binding site are well described by the observed electron density, suggesting that they are a good system in which to apply this approach to achieving selectivity. The achievement reported in this communication is illustrated most clearly by considering where compounds **8** and **9** would be found if added to the plots in Figure 1. They represent a good starting point for optimization toward a clinical candidate that is able to test the hypothesis that inhibition of FGFRs is of therapeutic value.

■ EXPERIMENTAL SECTION

Chemistry. All reactions were performed under inert conditions (nitrogen) unless otherwise stated. All solvents and reagents were purchased from commercial sources and used without further purification. Upon workup, organic solvents were typically dried prior to concentration with anhydrous MgSO₄ or Na₂SO₄. Flash silica chromatography was typically performed on an Isco Companion, using Silicycle silica gel, 230–400 mesh, 40–63 μm cartridges, Grace Resolv silica cartridges, or Isolute Flash Si or Si II cartridges. Reverse phase chromatography was performed using a Waters XBridge Prep C18 OBD column, 5 μm silica, 19 mm diameter, 100 mm length), using decreasingly polar mixtures of either water (containing 1% NH₃) and MeCN or water (containing 0.1% formic acid) and MeCN as eluents. Analytical LC–MS was performed on a Waters 2790 LC instrument with a 996 PDA and 2000 amu ZQ single quadrupole mass spectrometer using a Phenomenex Gemini 50 mm × 2.1 mm, 5 μm

C18 column, or UPLC was performed on an Waters Acquity binary solvent manager with Acquity PDA and an SQD mass spectrometer using a 50 mm × 2.1 mm, 1.7 μm BEH column from Waters, and purities were measured by UV absorption at 254 nm and are ≥95% unless otherwise stated. NMR spectra were recorded on a Bruker Av400 or Bruker DRX400 spectrometer at 400 MHz in DMSO-*d*₆ at 303 K unless otherwise indicated. ¹H NMR spectra are reported as chemical shifts in parts per million (ppm) relative to an internal solvent reference.

N4-(3-(3,5-Dimethoxyphenethyl)-1H-pyrazol-5-yl)-N2-((3-methylisoxazol-5-yl)methyl)pyrimidine-2,4-diamine, 9. Hydrogen chloride, 4 M in dioxane (2–3 drops), was added to 3-(3,5-dimethoxyphenethyl)-1H-pyrazol-5-amine (286 mg, 1.16 mmol) and 4-chloro-*N*-((3-methylisoxazol-5-yl)methyl)pyrimidin-2-amine (200 mg, 0.89 mmol) in EtOH (10 mL). The solution was heated at reflux for 20 h and then allowed to cool to room temperature. The solid product was collected by filtration, washed with EtOH, and dried under vacuum to afford the crude product as the HCl salt. The solid was then triturated with MeOH/H₂O (~1:1 mixture) and basified with 7 M NH₃ in MeOH, causing the material to go into solution briefly and then precipitate out again. The solid was collected by filtration, washed with a little MeOH followed by water, and then dried under vacuum to afford the title compound as a pale cream solid (288 mg, 74%). ¹H NMR (400 MHz, DMSO/CD₃COOD, 30 °C) 2.16 (3H, s), 2.83 (4H, s), 3.70 (6H, s), 4.55 (2H, s), 6.11 (1H, s), 6.18 (1H, bs), 6.27 (1H, bs), 6.31 (1H, t), 6.40 (2H, d), 7.83 (1H, d); ¹³C NMR (500 MHz, DMSO/CD₃COOD, 100 °C) 10.6, 27.1, 34.9, 36.9, 55.1, 94.5, 96.7, 98.4, 102.0, 106.7, 143.5, 144.1, 146.5, 155.5, 159.1, 160.2, 160.7, 161.4, 171.2. HRMS (ESI): calcd for C₂₂H₂₅N₇O₃, 436.20916; found, 436.20886. Anal. Calcd for C₂₂H₂₅N₇O₃: C, 60.68; H, 5.79; N, 22.51. Found: C, 60.32, H, 5.80; N, 22.34.

N4-(3-(3,5-Dimethoxyphenethyl)-1H-pyrazol-5-yl)-N2-((3-methylisoxazol-5-yl)methyl)pyrimidine-2,4-diamine, compound 8 (100 mg), was purified by preparative HPLC (Waters XBridge Prep C18 OBD column, 5 μm silica, 19 mm diameter, 100 mm length), using decreasingly polar mixtures of water (containing 1% NH₃) and MeCN as eluents. Fractions containing the desired compound were evaporated to afford the title compound (53 mg) as a white solid. Mp 170.3–170.5 °C; ¹H NMR (400 MHz, DMSO, 21 °C) 2.16 (3H, s), 2.82 (4H, s), 3.71 (6H, s), 4.53 (2H, s), 6.11 (1H, s), 6.21 (2H, bs), 6.31 (1H, t), 6.41 (2H, d), 7.83 (1H, d). Anal. Calcd for C₂₂H₂₅N₇O₃: C, 60.68; H, 5.79; N, 22.51. Found: C, 60.60, H, 5.74; N, 22.70.

3-(3,5-Dimethoxyphenylethyl)-1H-pyrazol-5-amine, used as starting material, was prepared as follows: (a) MeCN (2.29 mL, 43.61 mmol) was added to a slurry of sodium hydride (1.75 g dispersion in mineral oil, 43.61 mmol) in anhydrous toluene (70 mL) and the mixture stirred at room temperature for 30 min. Ethyl 3-(3,5-dimethoxyphenyl)propanoate (8.66 g, 36.34 mmol) in toluene (60 mL) was added, and the reaction mixture was heated at reflux for 18 h. After the mixture was cooled and the reaction quenched with a small amount of water, the solvent was evaporated under reduced pressure. The residue was dissolved in 2 M HCl (50 mL). The acidic solution was then extracted twice with EtOAc. The organic extracts were combined, washed with water followed by brine, and then dried over magnesium sulfate. After filtering, the solvent was evaporated under reduced pressure to yield the crude product as a yellow oil. The oil was purified by flash chromatography on silica, eluting with DCM. Fractions containing pure product were combined and evaporated to leave a cream solid (3.76 g, 44%). To the solid (3.72 g, 15.96 mmol) in EtOH (55 mL) was added hydrazine hydrate (852 μL, 17.56 mmol). The mixture was heated at reflux for 24 h before allowing it to cool. After the mixture was evaporated under reduced pressure, the residue was dissolved in DCM, washed with water followed by brine, dried with magnesium sulfate, filtered, and then evaporated under reduced pressure to afford 3-(3,5-dimethoxyphenylethyl)-1H-pyrazol-5-amine as a pale yellow solid (3.76 g, 42% over two steps). ¹H NMR (300.132 MHz, DMSO) δ 2.64–2.82 (4H, m), 3.71 (6H, s), 4.07–4.72 (2H, m), 5.20 (1H, s), 6.31 (1H, t), 6.38 (2H, d). MS: *m/z* 248 (MH⁺). **4-Chloro-*N*-((3-methylisoxazol-5-yl)methyl)pyrimidin-2-amine** was prepared as follows: To a solution containing 2-[(3-methylisoxazol-5-

yl)methylamino]pyrimidin-4-ol (8.8 g, 43.52 mmol) and diisopropylethylamine (9.6 mL) in toluene (40 mL) was added phosphorus oxychloride (4.8 mL, 51.50 mmol) dropwise. The gummy suspension was heated at 80 °C for 2 h. The mixture was allowed to cool to room temperature and then poured portionwise into saturated sodium bicarbonate solution. The product was extracted with EtOAc (×2), washed with brine, dried over magnesium sulfate, filtered, and then evaporated to leave a cream solid. The solid was washed with EtOAc and DCM (plus a few drops of MeOH), and the suspension was heated to reflux. After filtration, the product was obtained as a cream solid (1.6 g). The filtrate was loaded onto a silica column and then eluted with EtOAc. Fractions containing product were combined and then evaporated. The residue was triturated with Et₂O to afford 4-chloro-*N*-[(3-methylisoxazol-5-yl)methyl]pyrimidin-2-amine as a pale yellow solid (3.28 g). Total yield = 4.88 g (50%). ¹H NMR (400 MHz DMSO) 2.19 (s, 3H), 4.56 (d, 2H), 6.15 (s, 1H), 6.77 (d, 1H), 8.22 (t, 1H), 8.29 (d, 1H). MS: *m/z* 225 (MH⁺).

2-[(3-Methylisoxazol-5-yl)methylamino]pyrimidin-4-ol was prepared as follows: (3-Methylisoxazol-5-yl)methanamine (9.3 g, 83 mmol) and 2-methylsulfonylpyrimidin-4-ol (9.8 g, 69 mmol) were heated together at 160 °C for 4 h. The mixture was allowed to cool to room temperature and then dissolved in DCM and purified by flash chromatography on silica, eluting with a gradient of 5–15% MeOH in DCM. Fractions containing product were combined and evaporated to afford 2-[(3-methylisoxazol-5-yl)methylamino]pyrimidin-4-ol as a brown gum (8.88 g, 62%). ¹H NMR (400 MHz, DMSO) δ 2.19 (s, 3H), 4.57 (s, 2H), 5.6 (d, 1H), 6.19 (s, 1H), 7.03 (bs, 1H), 7.61 (d, 1H), 11 (bs, 1H). MS: *m/z* 207 (MH⁺).

Protein Expression and Purification. Human FGFR1 consisting of residues 458–765 was engineered to incorporate a TEV-cleavable N-terminal 6×His tag and mutations C488A and C584S.²⁷ Non-phosphorylated FGFR1 protein was obtained from 24 h growth of IPTG-induced *E. coli* BL21 (DE3) Star cells coexpressing the PTP1B phosphatase gene (induction at 20 °C using 100 μM IPTG). Following cell lysis in buffer consisting of 20 mM Tris-HCl, pH 7.8, 10 mM imidazole, 300 mM NaCl, 2 mM TCEP and clarification of the lysate by centrifugation, the FGFR1 protein was bound to a Ni-NTA column (QIAGEN), washed and step-eluted in 20 mM Tris-HCl, pH 7.8, 250 mM imidazole, 300 mM NaCl, 2 mM TCEP. The protein was subjected to TEV cleavage after exchange into 20 mM Tris-HCl, pH 7.8, 300 mM NaCl, 2 mM TCEP, 5 mM EDTA and further purified by ion-exchange chromatography after exchange into 20 mM Tris-HCl, pH 7.5, eluting bound protein with a 0–1 M NaCl gradient. The final purification step consisted of size-exclusion chromatography on a Superdex 200 column pre-equilibrated and run in 20 mM Tris-HCl, pH 8.0, 20 mM NaCl, 2 mM TCEP buffer followed by concentration to 10 mg/mL. The FGFR1 protein purity was assessed by SDS–PAGE and the predicted molecular mass confirmed by liquid chromatography–mass spectrometry. Purified protein was snap frozen in liquid nitrogen and stored at –80 °C for later use in crystallization.

Crystallization and Data Collection. Crystals of FGFR1 were grown at 4 °C using the hanging drop vapor diffusion method from a reservoir solution of 16–20% PEG 8000, 100 mM PCTP, pH 6.25–7.25, 100–300 mM (NH₄)₂SO₄, 25% ethylene glycol. Crystals appear after 4 days and need a further 7 days to reach the final dimensions of approximately 100 μm × 20 μm × 20 μm. Crystals were then subjected to cross-linking with glutaraldehyde²⁸ and transferred into a soaking solution containing 98% (v/v) reservoir solution and 2% (v/v) DMSO, to which compounds 1, 6, and 8 were added independently of each other to a final concentration of 2 mM. Soaks were carried out at 4 °C for 6 h, after which the crystals were flash frozen in liquid nitrogen. Diffraction data were collected in-house on a Rigaku FRE rotating anode generator equipped with a Saturn 944 CCD detector or at the ESRF on beamline ID23-1, processed using MOSFLM^{29,30} and scaled and merged using SCALA as implemented in the CCP4 software package.³¹ The FGFR1-compound crystals belong to space group C2 (Table S1 in Supporting Information) and contain two complexes per asymmetric unit. The structures were solved by molecular replacement using AMORE using the structure of FGFR1 (PDB code 1FGK) as the search model.³² A number of iterations of

model-building, using the $2F_o - F_c$ and $F_o - F_c$ electron density maps as displayed in COOT,³³ followed by refinement in REFMAC³⁰ were carried out to produce the final structures (PDB codes 4F63, 4F64, and 4F65). All structural figures were made using PyMOL.³⁴

Biological Evaluation. In all enzyme and cell assays, compound was tested at a range of concentrations. The mean data values for each concentration, along with untreated control wells and 100% inhibition/competition control wells, were used to derive a plot of inhibition/competition against concentration. Origin software was used to interpolate IC₅₀ values by nonlinear regression.

Kinase Inhibition Assays Using Caliper Technology. The inhibitory activity of compound against the kinases FGFR1, KDR, and IGF1R was determined with Caliper off-chip incubation mobility shift assays, using a microfluidic chip to measure the conversion of a fluorescent labeled peptide to a phosphorylated product. Custom peptide substrates with a fluorescent tag, sequence specific for each enzyme, were obtained from Cambridge Research Biochemicals (Cleveland, U.K.). Enzymes, peptide substrates, and ATP were incubated in the presence of compound diluted in DMSO (1% v/v DMSO assay final), in white Greiner 384-well low volume plates, in a total reaction volume of 12 μL. Enzymes and peptides were added separately to the compound plates and were incubated at room temperature, and the kinase reaction was then quenched with the addition of a stop buffer (comprising 100 mM HEPES (pH 7.5), 5% DMSO, 88 mM EDTA, 0.22% Caliper coating reagent no. 3, 0.033% Brij-35 solution). Stopped assay plates were then read using the Caliper LabChip LC3000.

GST-FGFR1 human recombinant kinase domain (residues 456–765) with an N-terminal GST-tag (expressed from a baculovirus in Sf21 insect cells) was obtained from Millipore. The kinase reaction [170 μM ATP, 5 nM enzyme, 1.5 μM substrate] in phosphorylation buffer (100 mM HEPES (pH 7.5), 5 mM MgCl₂, 1 mM DTT, 1 mM EDTA, 0.22% Caliper coating reagent no. 3, 0.033% Brij-35 solution) was quenched after a 40 min incubation.

GST-VEGFR2 (KDR) human recombinant kinase domain (residues 805–1356) with an N-terminal GST-tag (expressed from a baculovirus in Sf9 insect cells) was obtained from BPS Bioscience Inc. The kinase reaction (7 μM ATP, 8 nM enzyme, 1.5 μM substrate) in phosphorylation buffer (50 mM MOPS (pH 6.5), 20 mM MnCl₂, 4 mM DTT, 0.05% CHAPSO) was quenched after a 90 min incubation.

IGF-1R human recombinant kinase domain (residues 959 to end) containing an N-terminal His6-tag (expressed by baculovirus in Sf21 insect cells) was obtained from Upstate. The kinase reaction [7 μM (below *K_m*) ATP, 15 nM enzyme, 1.5 μM substrate] in phosphorylation buffer [50 mM MOPS (pH 6.5), 5 mM MnCl₂, 1 mM DTT, 0.004% Triton X-100] was quenched after an 80 min incubation.

Measurement of IGF-1R Phosphorylation. IGF-1R null murine fibroblasts R+ cells expressing human IGF-1R were from Xiao Tu (Kimmel Cancer Center, Thomas Jefferson University, Philadelphia, PA, U.S.). R+ cells were derived from transgenic mouse IGF1R knockouts that were then transfected with human insulin-like growth factor 1 receptor (IGF1R). R+ cells were routinely cultured in DMEM (Gibco) growth medium supplemented with 2 mM L-glutamine (Invitrogen), 10% (v/v) heat inactivated fetal calf serum (PAA), and hygromycin B (50 mg/mL) in a 5% CO₂ incubator at 37 °C. Cells were plated at a density of 5 × 10³ cells per well in 96-well black Packard View plates (PerkinElmer) in DMEM supplemented with 1% heat inactivated FCS and 1% L-glutamine and incubated at 37 °C. Following overnight culture cells were acoustically dosed using an Echo 555 (Labcyte), with compounds serially diluted in 100% DMSO. Following a 30 min compound treatment cells were stimulated for 20 min with a final concentration of 30 nM IGF-1 (Groppe's IMOOI) diluted in DMEM without serum. Cells were fixed with 4% formaldehyde for 20 min and treated with 0.05% Triton for 10 min. Cells were then blocked with 2% bovine serum albumin (BSA) and 2% goat serum (DAKO Ltd.) in PBS for 1 h and incubated with rabbit dual phospho specific anti-phospho IGF-1R/IR antibody (Biosource) (1:350) for 1 h, followed by incubation with anti-rabbit Alexa Fluor 488 secondary antibody (1:1000) for 1 h. Measurement was done

using an Acumen Explorer HTS reader (TTP Labtech Ltd.) at excitation wavelength of 488 nm and emission wavelength of 530 nm.

Measurement of InsR Phosphorylation. CHOT cells over-expressing human insulin receptor were obtained from Dr. J. Tavaré (Department of Biochemistry, University of Bristol, Bristol, U.K.). CHOT cells were routinely cultured in Ham F12 (Invitrogen) growth medium supplemented with 2 mM L-glutamine (Invitrogen), 10% (v/v) heat inactivated fetal calf serum (PAA Laboratories), and hygromycin B (50 µg/mL) in a 5% CO₂ incubator at 37 °C. Cells were plated at a density of 5 × 10³ cells per well in 96-well black Packard View plates (PerkinElmer) in DMEM supplemented with 1% heat inactivated FCS and 1% L-glutamine and incubated at 37 °C. Following overnight culture, cells were acoustically dosed using an Echo 555 (Labcyte), with compounds serially diluted in 100% DMSO. Following a 60 min compound treatment cells were stimulated for 20 min with a final concentration of 30 nM insulin ligand (Sigma), diluted in Ham F12 without serum. Cells were fixed with 4% formaldehyde for 20 min and treated with 0.05% Triton for 10 min. Cells were then blocked with 2% bovine serum albumin (BSA) and 2% goat serum (DAKO Ltd.) in PBS for 30 min and incubated with rabbit anti-phospho InsR antibody (AZ proprietary) overnight, followed by incubation with anti-rabbit Alexa Fluor 488 secondary antibody for 1 h. Measurement was done using an Acumen Explorer HTS reader (TTP Labtech Ltd.) at excitation wavelength of 488 nm and emission wavelength of 530 nm.

Measurement of FGFR1 Phosphorylation. Cos-1 cells were routinely cultured in DMEM growth medium supplemented with 2 mM L-glutamine and 3% fetal calf serum (FCS). For transfection, Lipofectamine 2000 (Invitrogen) was mixed with OptiMEM (Invitrogen) and incubated at room temperature for 5 min. DNA encoding 3'FLAG FGFR1 or empty vector (pcDNA3.2) was diluted with OptiMEM, and equal volumes of DNA and Lipofectamine 2000 were combined (DNA/lipid = 1:1.2 ratio) and incubated at room temperature for 20 min. Harvested cells were diluted with 1% FCS/DMEM. The complexed transfection solution was added to the cell solution, and the cells were seeded at 1.2 × 10⁴ cells per well in 96-well plates (Costar) and incubated at 37 °C in a 5% CO₂ incubator overnight. The following day cells were acoustically dosed using an Echo 555 (Labcyte), with compounds serially diluted in 100% DMSO. Following a 1 h incubation, medium was removed and cells were fixed with 100% methanol and incubated for 20 min and then treated with 0.1% Triton for 20 min. Cells were then incubated with monoclonal anti-phospho-FGFR antibody (Cell Signaling Technology) (1:1000) for 1 h followed by incubation with anti-mouse Alexa Fluor 594 secondary antibody (1:500) and Hoechst (1:1000) for 1 h. Measurement was done using an Arrayscan (Cellomics).

Measurement of KDR Phosphorylation. HUVECs were obtained from Promocell and cultured in MCDB131 (Gibco) growth medium supplemented with 2 mM glutamine, 10% FCS, and 1% penicillin–streptomycin (Gibco) in a 5% CO₂ incubator at 37 °C. Cells were plated at a density of 3.5 × 10⁴ cells per well in 24-well plates in MCDB131 medium supplemented with 2 mM glutamine, 1% FCS, and 1% penicillin–streptomycin. After overnight incubation, the medium was replaced with 500 µL of serum free medium. Compounds were added 150 min later (diluted in DMSO to a final concentration of 10 mM) and incubated for 90 min before stimulation with VEGF (25 ng/well) for 5 min. Cells were lysed with RIPA buffer (60 mM Tris, pH 7.4, 150 mM NaCl, 1 mM EDTA, 10× RIPA detergent (10% NP40 + 2.5% deoxycholate), and phosphatase inhibitor cocktails 1 (Sigma P2850) and 2 (Sigma P5726) and protease inhibitor (Sigma P8340)). Lysates were then developed according to the human phospho-VEGF R2 (KDR) ELISA protocol (R&D Systems) until the plate development stage where SuperSignal (Pierce) was used. Luminescence measurement was carried out using a Tecan plate reader.

All IC₅₀ values were transformed to pIC₅₀ values, and an average of at least three values for enzyme data and at least two values for cellular data is reported in the tables other than for cellular data for KDR where only one measurement was made on all compounds other than

9, which was studied in duplicate. Individual values of IC₅₀ are provided in the Supporting Information.

Percentage inhibition data were obtained at the concentrations mentioned in the text from the National Centre for Protein Kinase Profiling at the University of Dundee, U.K.

■ ASSOCIATED CONTENT

📄 Supporting Information

Crystallographic parameters, individual IC₅₀ and pIC₅₀ values, and sequence overlays and percentage inhibition for other kinases. This material is available free of charge via the Internet at <http://pubs.acs.org>.

Accession Codes

The crystal structures of compounds 1, 6, and 8 in complex with FGFR have been deposited with the RCSB Protein Data Bank under accession codes 4F63, 4F64, and 4F65, respectively.

■ AUTHOR INFORMATION

Corresponding Author

*Phone: +44 1625 231853. E-mail: andrew.leach@astrazeneca.com.

Notes

The authors declare no competing financial interest.

■ ACKNOWLEDGMENTS

The authors thank Jason Kettle, Julie Tucker, and Ray Gairns for assistance in the preparation of this manuscript and many co-workers for contributions to the FGF project.

■ ABBREVIATIONS USED

FGFR, fibroblast growth factor receptor (usually referring here to its tyrosine kinase domain/activity) unless indicated as FGFR1. FGFR is used to refer collectively to the four isoforms FGFR1–4; KDR, kinase insert domain receptor (VEGFR2); IGF1R, insulin-like growth factor I receptor; InsR, insulin receptor tyrosine kinase; ATP, adenosine triphosphate; IPTG, isopropyl β-D-thiogalactoside; TCEP, tris(carboxyethyl)-phosphine; EDTA, ethylenediaminetetraacetic acid; SDS–PAGE, sodium dodecyl sulfate polyacrylamide gel electrophoresis; PCTP, propionic acid, cacodylate, bis-Tris propane; PEG, polyethylene glycol; HEPES, 4-(2-hydroxyethyl)-1-piperazineethanesulfonic acid; MOPS, 3-(N-morpholino)-propanesulfonic acid; DTT, dithiothreitol; DMEM, Dulbecco's modified Eagle's medium; PBS, phosphate buffered saline

■ REFERENCES

- (1) Aronov, A. M.; Murcko, M. A. Toward a Pharmacophore for Kinase Frequent Hitters. *J. Med. Chem.* **2004**, *47*, 5616–5619.
- (2) Bamborough, P.; Drewry, D.; Harper, G.; Smith, G. K.; Schneider, K. Assessment of Chemical Coverage of Kinome Space and Its Implications for Kinase Drug Discovery. *J. Med. Chem.* **2008**, *51*, 7898–7914.
- (3) Fabian, M. A.; Biggs, W. H., 3rd; Treiber, D. K.; Atteridge, C. E.; Azimioara, M. D.; Benedetti, M. G.; Carter, T. A.; Ciceri, P.; Edeen, P. T.; Floyd, M.; Ford, J. M.; Galvin, M.; Gerlach, J. L.; Grotzfeld, R. M.; Herrgard, S.; Insko, D. E.; Insko, M. A.; Lai, A. G.; Lelias, J.; Mehta, S. A.; Milanov, Z. V.; Velasco, A. M.; Wodicka, L. M.; Patel, H. K.; Zarrinkar, P. P.; Lockhart, D. J. A small molecule-kinase interaction map for clinical kinase inhibitors. *Nat. Biotechnol.* **2005**, *23*, 329–336.
- (4) Posy, S. L.; Hermsmeier, M. A.; Vaccaro, W.; Ott, K.; Todderud, G.; Lippy, J. S.; Trainor, G. L.; Loughney, D. A.; Johnson, S. R. Trends in Kinase Selectivity: Insights for Target Class-Focused Library Screening. *J. Med. Chem.* **2011**, *54*, 54–66.

- (5) Xing, L.; Shieh, H. S.; Selness, S. R.; Devraj, R. V.; Walker, J. K.; Devadas, B.; Hope, H. R.; Compton, R. P.; Schindler, J. F.; Hirsch, J. L.; Benson, A. G.; Kurumbail, R. G.; Stegeman, R. A.; Williams, J. M.; Broadus, R. M.; Walden, Z.; Monahan, J. B. Structural Bioinformatics-Based Prediction of Exceptional Selectivity of p38 MAP Kinase Inhibitor PH-797804. *Biochemistry* **2009**, *48*, 6402–6411.
- (6) Vieth, M.; Higgs, R. E.; Robertson, D. H.; Shapiro, M.; Gragg, E. A.; Hemmerle, H. Kinomics—Structural Biology and Chemogenomics of Kinase Inhibitors and Targets. *Biochim. Biophys. Acta* **2004**, *1697*, 243–257.
- (7) Liao, J. J. Molecular Recognition of Protein Kinase Binding Pockets for Design of Potent and Selective Kinase Inhibitors. *J. Med. Chem.* **2007**, *50*, 409–424.
- (8) Verkhivker, G. M. Exploring Sequence-Structure Relationships in the Tyrosine Kinome Space: Functional Classification of the Binding Specificity Mechanisms for Cancer Therapeutics. *Bioinformatics* **2007**, *23*, 1919–1926.
- (9) Verkhivker, G. M. Computational Proteomics of Biomolecular Interactions in the Sequence and Structure Space of the Tyrosine Kinome: Deciphering the Molecular Basis of the Kinase Inhibitors Selectivity. *Proteins: Struct., Funct., Bioinf.* **2007**, *66*, 912–929.
- (10) McInnes, C.; Fischer, P. M. Strategies for the Design of Potent and Selective Kinase Inhibitors. *Curr. Pharm. Des.* **2005**, *11*, 1845–1863.
- (11) Caffrey, D. R.; Lunney, E. A.; Moshinsky, D. J. Prediction of Specificity-Determining Residues for Small-Molecule Kinase Inhibitors. *BMC Bioinf.* **2008**, *9*, 491.
- (12) Zuccotto, F.; Ardini, E.; Casale, E.; Angiolini, M. Through the “Gatekeeper Door”: Exploiting the Active Kinase Conformation. *J. Med. Chem.* **2010**, *53*, 2681–2694.
- (13) Weiss, M. M.; Harmange, J.; Polverino, A. J.; Bauer, D.; Berry, L.; Berry, V.; Borg, G.; Bready, J.; Chen, D.; Choquette, D.; Coxon, A.; DeMelfi, T.; Doerr, N.; Estrada, J.; Flynn, J.; Graceffa, R. F.; Harriman, S. P.; Kaufman, S.; La, D. S.; Long, A.; Neervannan, S.; Patel, V. F.; Potashman, M.; Regal, K.; Roveto, P. M.; Schrag, M. L.; Starnes, C.; Tasker, A.; Teffera, Y.; Whittington, D. A.; Zanon, R. Evaluation of a Series of Naphthamides as Potent, Orally Active Vascular Endothelial Growth Factor Receptor-2 Tyrosine Kinase Inhibitors. *J. Med. Chem.* **2008**, *51*, 1668–1680.
- (14) Vulpetti, A.; Crivori, P.; Cameron, A.; Bertrand, J.; Brasca, M. G.; D’Alessio, R.; Pevarello, P. Structure-Based Approaches to Improve Selectivity: CDK2-GSK3 β Binding Site Analysis. *J. Chem. Inf. Model.* **2005**, *45*, 1282–1290.
- (15) Noble, M. E. M.; Endicott, J. A.; Johnson, L. N. Protein Kinase Inhibitors: Insights into Drug Design from Structure. *Science (Washington, DC, U. S.)* **2004**, *303*, 1800–1805.
- (16) Morphy, R. Selectively Nonselective Kinase Inhibition: Striking the Right Balance. *J. Med. Chem.* **2010**, *53*, 1413–1437.
- (17) Barlaam, B.; Pape, A.; Thomas, A. PCT Patent 2003048133, 2003.
- (18) Turner, N.; Grose, R. Fibroblast growth factor signalling: from development to cancer. *Nat. Rev. Cancer* **2010**, *10*, 116–129.
- (19) Mohammadi, M.; Froum, S.; Hamby, J. M.; Schroeder, M. C.; Panek, R. L.; Lu, G. H.; Eliseenkova, A. V.; Green, D.; Schlessinger, J.; Hubbard, S. R. Crystal Structure of an Angiogenesis Inhibitor Bound to the FGF Receptor Tyrosine Kinase Domain. *EMBO J.* **1998**, *17*, 5896–5904.
- (20) Mohammadi, M.; McMahon, G.; Sun, L.; Tang, C.; Hirth, P.; Yeh, B. K.; Hubbard, S. R.; Schlessinger, J. Structure of the Tyrosine Kinase Domain of Fibroblast Growth Factor Receptor in Complex with Inhibitors. *Science (Washington, D.C.)* **1997**, *276*, 955–960.
- (21) Hubbard, S. R.; Wei, L.; Ellis, L.; Hendrickson, W. A. Crystal structure of the tyrosine kinase domain of the human insulin receptor. *Nature (London)* **1994**, *372*, 746–754.
- (22) Harris, P. A.; Cheung, M.; Hunter, R. N., III; Brown, M. L.; Veal, J. M.; Nolte, R. T.; Wang, L.; Liu, W.; Crosby, R. M.; Johnson, J. H.; Epperly, A. H.; Kumar, R.; Luttrell, D. K.; Stafford, J. A. Discovery and Evaluation of 2-Anilino-5-aryloxazoles as a Novel Class of VEGFR2 Kinase Inhibitors. *J. Med. Chem.* **2005**, *48*, 1610–1619.
- (23) Dimitroff, C. J.; Klohs, W.; Sharma, A.; Pera, P.; Driscoll, D.; Veith, J.; Steinkampf, R.; Schroeder, M.; Klutchko, S.; Sumlin, A.; Henderson, B.; Dougherty, T. J.; Bernacki, R. J. Anti-Angiogenic Activity of Selected Receptor Tyrosine Kinase Inhibitors, PD166285 and PD173074: Implications for Combination Treatment with Photodynamic Therapy. *Invest. New Drugs* **1999**, *17*, 121–135.
- (24) Thompson, A. M.; Delaney, A. M.; Hamby, J. M.; Schroeder, M. C.; Spoon, T. A.; Crean, S. M.; Showalter, H. D. H.; Denny, W. A. Synthesis and Structure–Activity Relationships of Soluble 7-Substituted 3-(3,5-Dimethoxyphenyl)-1,6-naphthyridin-2-amines and Related Ureas as Dual Inhibitors of the Fibroblast Growth Factor Receptor-1 and Vascular Endothelial Growth Factor Receptor-2 Tyrosine Kinases. *J. Med. Chem.* **2005**, *48*, 4628–4653.
- (25) *clogP*, version 4.71; Daylight Chemical Information Systems: Santa Fe, NM.
- (26) Hansch, C.; Leo, A.; Unger, S. H.; Kim, K. H.; Nikaitani, D.; Lien, E. J. Aromatic Substituent Constants for Structure–Activity Correlations. *J. Med. Chem.* **1973**, *16*, 1207–1216.
- (27) Mohammadi, M.; Schlessinger, J.; Hubbard, S. R. Structure of the FGF Receptor Tyrosine Kinase Domain Reveals a Novel Autoinhibitory Mechanism. *Cell* **1996**, *86*, 577–587.
- (28) Lusty, C. J. A Gentle Vapor-Diffusion Technique for Crosslinking of Protein Crystals for Cryocrystallography. *J. Appl. Crystallogr.* **1999**, *32*, 106–112.
- (29) Batty, T. G. G.; Kontogiannis, L.; Johnson, O.; Powell, H. R.; Leslie, A. G. W. iMOSFLM: A New Graphical Interface for Diffraction-Image Processing with MOSFLM. *Acta Crystallogr., Sect. D: Biol. Crystallogr.* **2011**, *67*, 271–281.
- (30) Murshudov, G. N.; Vagin, A. A.; Dodson, E. J. Refinement of Macromolecular Structures by the Maximum-Likelihood Method. *Acta Crystallogr., Sect. D: Biol. Crystallogr.* **1997**, *53*, 240–255.
- (31) Bailey, S. The CCP4 Suite: Programs for Protein Crystallography. *Acta Crystallogr., Sect. D: Biol. Crystallogr.* **1994**, *50*, 760–763.
- (32) Navaza, J. AMoRe: An Automated Package for Molecular Replacement. *Acta Crystallogr., Sect. A: Found. Crystallogr.* **1994**, *50*, 157–163.
- (33) Emsley, P.; Cowtan, K. Coot: Model-Building Tools for Molecular Graphics. *Acta Crystallogr., Sect. D: Biol. Crystallogr.* **2004**, *60*, 2126–2132.
- (34) *The PyMOL Molecular Graphics System*, version 1.2r3pre; Schrödinger, LLC: New York.